Half-Heusler Alloy Characterization: $(Ti_{0.37}Zr_{0.37}Hf_{0.26})NiSn$

Group A

Antonin Cajka, Mahnaz Moradian, Martin Nyborg, Xinwei Sun

MENA/3100 – Characterization of Materials

Spring 2015

Abstract

We begin this report by presenting the structure and physical properties of half-Heusler alloys. After the theoretical part, the description of synthesis conditions of our sample (Ti0.37Zr0.37Hf0.26)NiSn follows. Details of phase identification and microstructure characterization are carried out utilizing different microscopic and spectroscopic methods. Bright-field imaging mode of light microscopy provided us the first view of the microstructure of our sample based on contrast due to differences in wave amplitudes.

Back scattering electron (BSE) image of scanning electron microscope (SEM) was used to examine the composition and distribution of Ti, Zr and Hf atoms. Multiphase behavior was observed. Simultaneously, we did element analysis by using X-ray energy-dispersive spectrometer (EDS). A closer look at the local structure and composition by X-ray power diffraction (XRD) (untreated/heated sample) revealed the coexistence of different half-Heusler phases, which is actually the case for all samples containing mixtures of *X*-elements.

Key words

Half-Heusler alloy, LM, X-ray powder diffraction analysis, SEM, EDX

Introduction

After the discovery of the first Heusler compound Cu2MnAl by Fritz Heusler in 1903, another group of materials – half-Heusler compounds has also aroused great interest in the field over the past decades, and lots of research is done around it. By changing the chemical composition of half-Heusler, their band gap can be adjusted from 0 – 4eV [i]. Thus, it is regarded as the promising thermoelectric material due to their good thermoelectric properties.

In principle, thermoelectricity is one possible way to convert waste heat directly into electricity [ii]. Consequently, the energy efficiency of any heat generating process can increase. Furthermore, half-Heusler is characterized as the potential alternative for future energy applications in solar cells. One problem remains for half-Heuslers: Their high lattice thermal conductivity [iii].

Characteristics

Half-Heusler compounds show semiconducting behavior, because they have 18 valence electrons. This causes a close-shell configuration [i]. Half-Heuslers are ternary compounds with 1:1:1 stoichiometry and a general formula of *XYZ*. In some half-Heulsers, *X* is a mixture of several elements. The mixture induces strong alloy scattering of phonons, and this will reduce the lattice thermal conductivity effectively [iv]. Besides, instead of a single phase, this gives rise to a complex distribution of half-Heusler phases with different ratios of X-metals [ii]. The ternary intermetallic half-Heusler alloys *X*NiSn, with nominal composition of (Ti$_{0.37}$Zr$_{0.37}$Hf$_{0.26}$)NiSn, has been investigated also in the past [iii,iv]. Half-Heusler materials belong to the class of thermoelectric and non-magnetic materials with the general formula of *XYZ* consisting of a covalent and an ionic part.

Structure of half-Heusler

As for in our case of $(Ti_{0.37}Zr_{0.37}Hf_{0.26})NiSn$, the electropositive element Ti was mixed with heavy elements Zr and Hf on the *X*-site. *Y* is a transition metal (Ni) and *Z* is the heavy main group element from the second half of the periodic table (Sn). In order to form the concentration ratio *X*:Ni:Sn as 1:1:1, all three electropositive elements Ti, Zr and Hf are divided in the corresponding ratio 0.37:0.37:0.26. The most electropositive elements *X* (Ti, Zr and Hf) is placed at the beginning of the formula, while the most electronegative element *Z* (Sn) at the end. *X* and *Y* atoms act as the cationic counterpart of the compound, and *Z* (Sn) has a unique anionic character.

Both full-Heusler and half-Heusler consists of 4 interpenetrating fcc lattices. Half-Heusler structure differs from the Heusler structure by filling of the vacant tetrahedral site and we gain the Cl_b structure. Half-Heusler phases crystallize in the cubic MgAgAs-type structure corresponding to the space group *F-43m*, no. 216, Cl_b [i]. *X*, *Y*, *Z* atoms form the three interpenetrating face-centered-cubic (fcc) sublattice where the main group *Z* with the electropositive *X* metals is occupying the octahedral holes, and the transition metal *Y* occupies half of the tetrahedral environment. This leads to a formation of NaCl-type lattice of *XZ* and a ZnS-type lattice of *YZ*, as shown in the Figure 1.
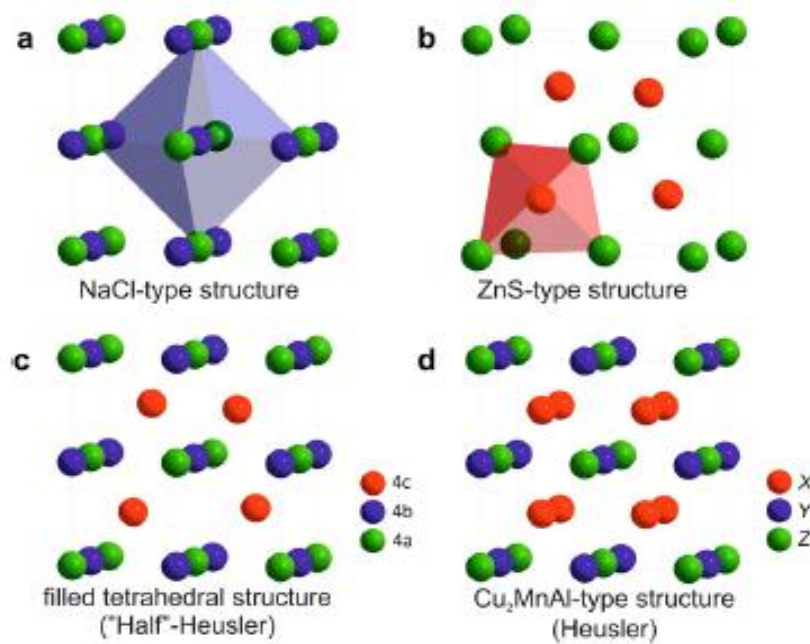

Figure 1 Half-Heusler materials are sum of NaCl-type (ionic) and the ZnS-type (covalent) lattice [i].

Within the lattice, we see that the Wyckoff positions *4a* (0, 0, 0) and *4c* (¼, ¼, ¼) form the covalent ZnS-type lattice (*Y–Z*), while the third atom occupies the octahedral vacancies in the ZnS-type lattice *4b* (½, ½, ½) and build up the ionic NaCl-type lattice (*X–Z*), showing a strong ionic character [v]. As for our sample $(Ti_{0.37}Zr_{0.37}Hf_{0.26})NiSn$, the Ni with intermediate electronegativity and the anionic Sn form the covalent ZnS-sublattice, while the most electropositive element *X* = $(Ti_{0.37}Zr_{0.37}Hf_{0.26})$ together with the most electronegative Sn built up for the NaCl-type substructure. As a result, four Sn atoms and four *X* = (Ti, Zr, Hf) atoms coordinate the Ni atom in form of an ideal cube. This atomic arrangement causes strong hybridization of d states of the *X* and *Y* atoms [vi] and furthermore generates a band gap 0.1 – 0.2 eV at Fermi [iii].

The sample is usually prepared by arc-melting (specifications follows in the Synthesis chapter). This is the high temperature process and during the rapid solidification, the compound is separated into two phases. These two phases grow dendritic. This microstructure is temperature resistant and decreases the thermal conductivity a lot, which again leads to higher thermoelectric efficiency.

Fast cooling leads to high strain in the material. This is due to changes in composition and lattice defects - point defects, dislocations, formation of non-equilibrium phases. The rapid cooling also results in uneven distribution of impurity phases, as the diffusion distances decrease. All these consequences, which result from the cooling process, decide the material's properties.

All in all, the microstructure of the material is changed during the cooling or solidification process. When the cooling happens fast, the solidification front is unstable and this leads to the formation of dendrites. The solidifying particles are originally spherical, but by rapid cooling, they develop arms; that makes it easier to carry away the heat. The formation of dendrites introduces new strain in the material, this reduces the thermal conductivity, and thus the thermoelectric efficiency is increased.

Synthesis of $(Ti_{0.37}Zr_{0.37}Hf_{0.26})NiSn$ half-Heusler

The main challenge is that this compound consists of many high melting point elements, Hf: 2233°C, Zr: 1855°C, Ti: 1666°C, Ni: 1455°C etc. Thus, a high temperature alloying method is needed. Because of that, the sample of composition $(Ti_{0.37}Zr_{0.37}Hf_{0.26})NiSn$ was prepared by arc-melting of stoichiometric amounts of mixed metals under an argon (Ar) atmosphere, followed by ball milling and annealing. The starting materials titanium (Ti), zirconium (Zr), hafnium (Hf), nickel (Ni) metal, tin (Sn) metal were well mixed and encapsulated in a silica or quartz tube, and then heat treated up to 850-900°C for several days. Because of Sn has high vapor pressure, some of it could have been evaporated during the high temperature arc melting (sample 1).

Consequently, a part of the sample was annealed at 850°C for 1 week. This should have significantly reduced the presence of impurity phases (more at XRD part). The sample after the annealing is considered as sample 2 in this report.

Results and Discussion

Morphology analysis

In order to determinate the morphology of the sample, two different methods was used in our study:

- Light optical microscopy
- Scanning electron microscopy (SEM)

Light optical microscopy should provide us the first view about the morphology of our sample and its behavior while, whereas the scanning electron microscopy should tell as more about details in the present phases, phase boundaries and distribution of elements along the surface.

Light microscopy

Sample preparation procedure

The sample was prepared for light microscopy by sectioning it in two by abrasive cutting with a diamond saw. Further, a cold mounting of the specimen (sample 1) was done in order to get a regular shape of the sample, which allows us to handle the sample while grinding and polishing. The purpose here was to make the surface of the specimen flat and remove surface damages caused by the cutting.

The one-half of the specimen was taken and hand-grinded with 1000 and 2000 grit paper by using of a simple hand grinding device. The resulting structure was checked after each step by the light microscopy. The results are presented in the Figure 2. The circle seen in the Figure 2a is a water droplet; we used water to cool down the sample during the grinding process. The second step was using the 4000 grit paper (Figure2b). Damage from the final grinding can be removed by polishing with the finest paper containing the diamond particles with the diameter about 2 µm; in order to make it a flat and scratch-free (Figure 2c). After the finest polishing, we can recognize the phase boundaries as well as also some pores in the picture.
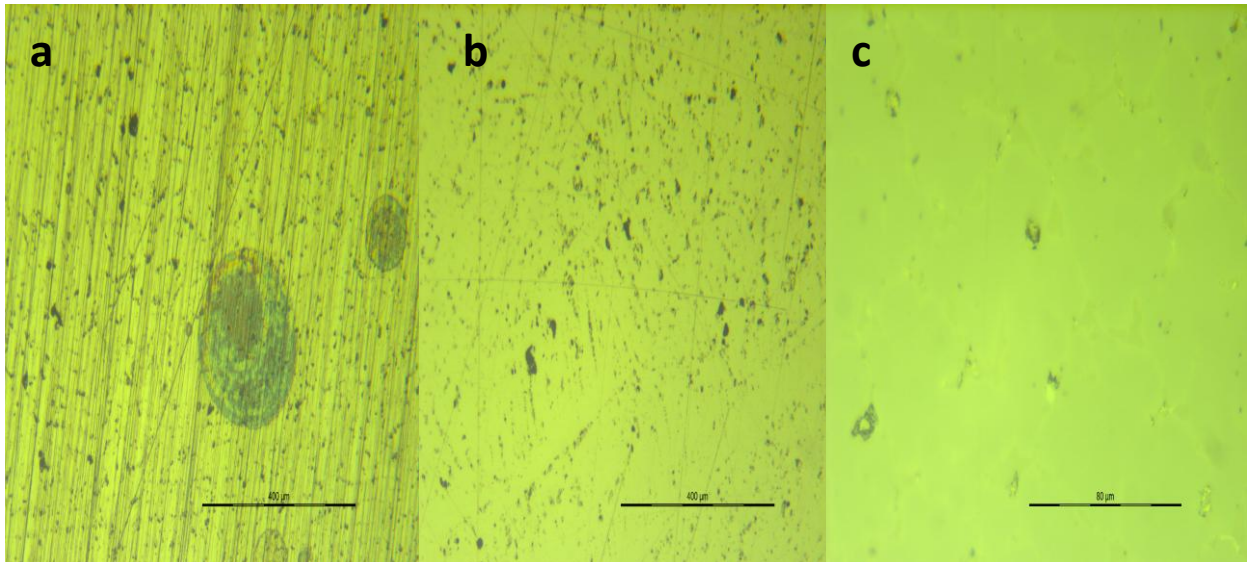

Figure 2 The sample surface during the grinding and polishing after the (a) 1000 grinding, (b) 4000 grinding and (c) finest paper polishing

Also the dendrite structures were observed by Nomarski microscopy in this place; as is shown in the Figure 3. It tells us that we have at least two phases growing separately along the sample volume. The further investigation follows in further chapters.
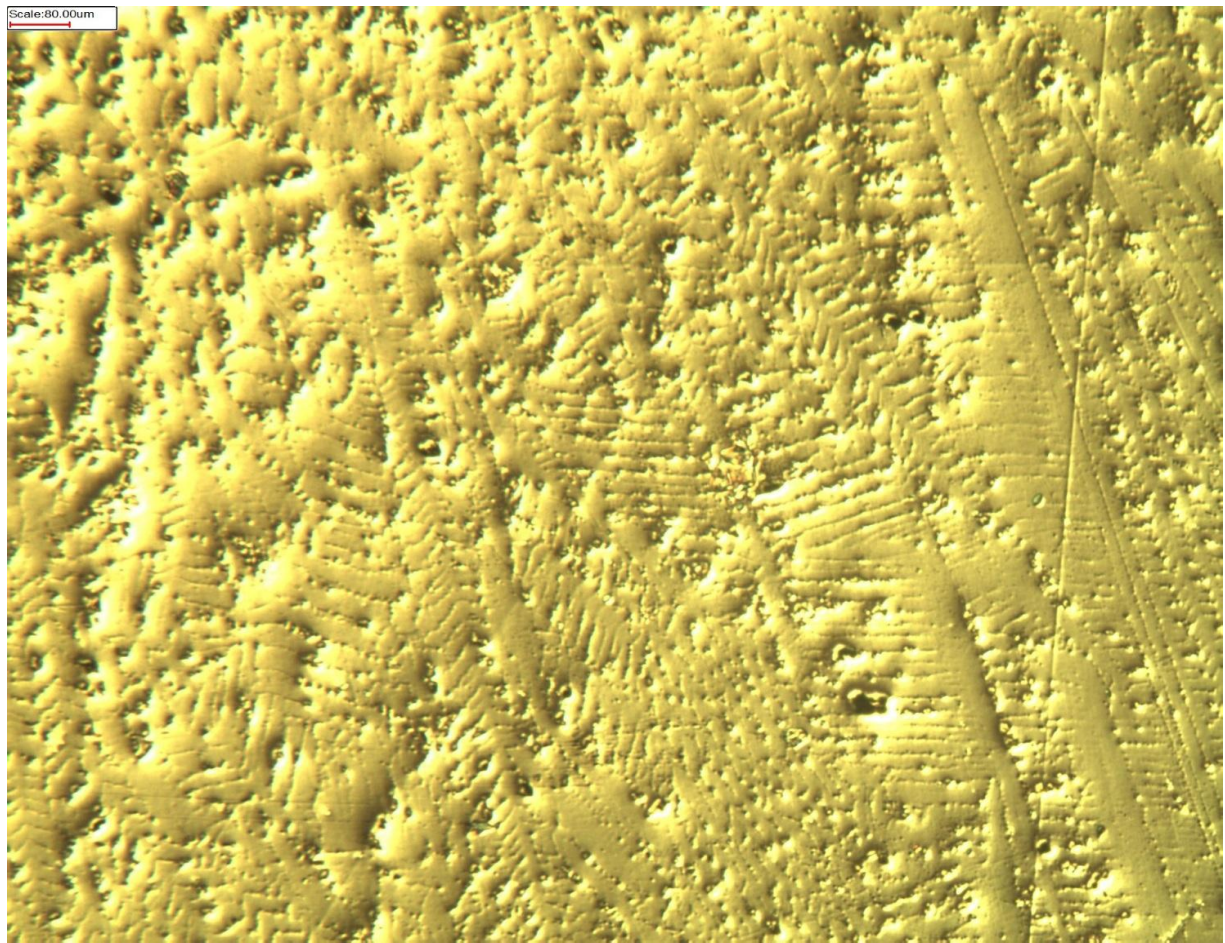
Figure 3 The Nomarski microscopy picture of the dendrite growth in our sample.

Scanning electron microscopy

In addition to the light microscopy, scanning electron microscopy analysis was done. First, we used the basic Table Top SEM (Hitachi TM3000) with the W-thread as an electron source and in high vacuum mode. The usual accelerating voltage was set up as 15 keV. The working distance varied in the interval from 7 to 11 mm. Also, the compatible mode using both secondary and back scattered electrons was used. Before the analysis, the sample had to be coated by carbon, and also the cuprum plate had to be attached - because of the charging of the sample surface by the incoming electron beam. The representative results are shown in the Figure 4 and 5.
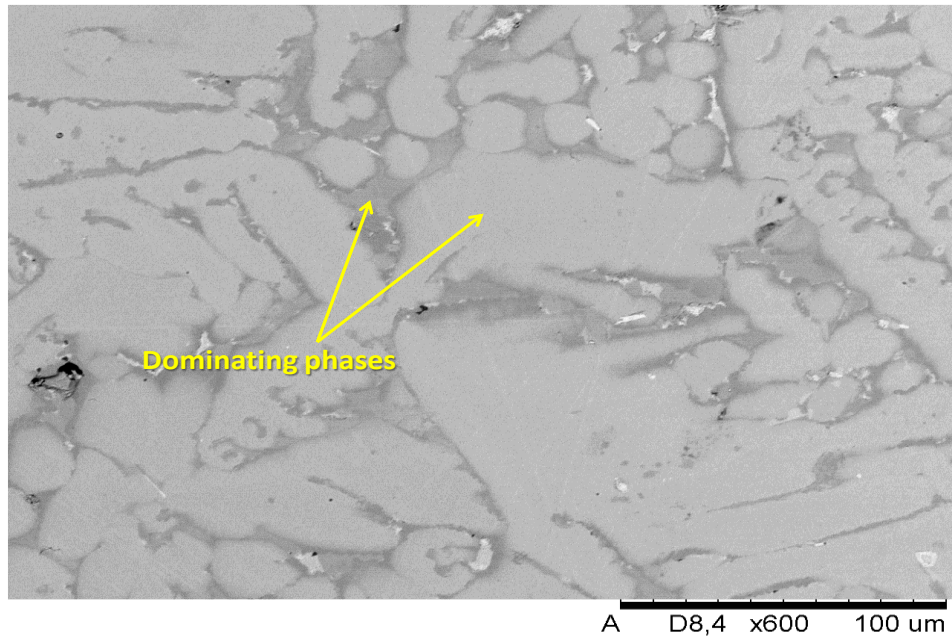
A   D8,4   x600   100 um

Figure 4 Table SEM picture of expected (Ti$_{0.37}$Zr$_{0.37}$Hf$_{0.26}$)NiSn in the middle area of the sample.

From SEM picture in the Figure 4 we can see approximately six phases having different chemical compositions distributed along whole sample. We can also see two dominating phases – light grey and dark grey areas. The surface of the sample is almost perfectly flat with the negligible presence of line scratches (consequence of imperfect polishing). In the Figure 5 we can see the SEM picture of the phase boundaries in the closest area to the edge of the sample.

A   D7,0   x800   100 um
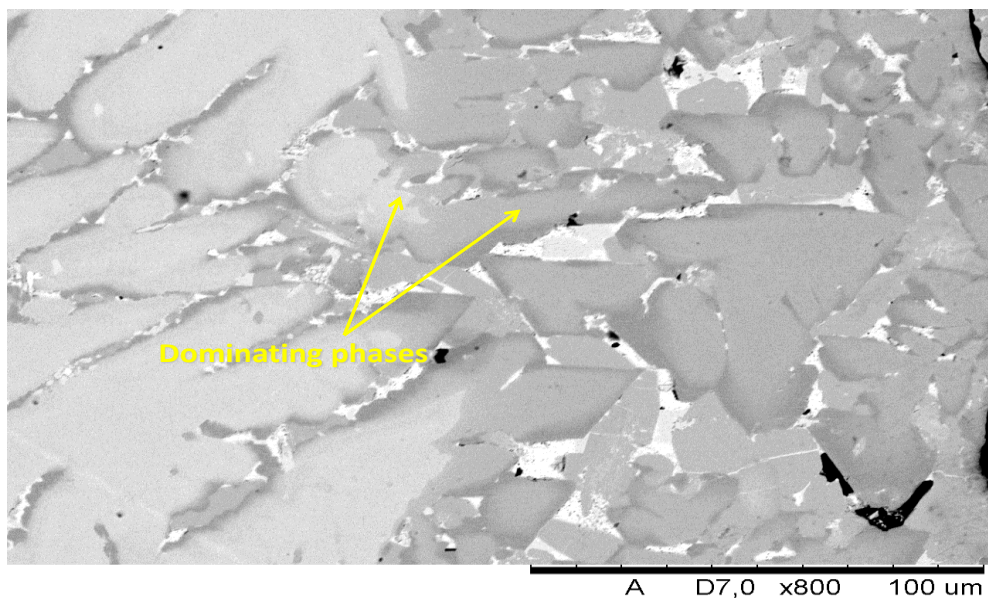
Figure 5 Table SEM picture of expected (Ti$_{0.37}$Zr$_{0.37}$Hf$_{0.26}$)NiSn in the edge area – variation of dominating phase and its boundaries.

We are also observing the significant difference in the chemical composition compared to the middle area of the sample. The effect of a different brightness (slight changes in the colour performance for the same phases) is noticeable. On this place, also the chemical analysis by using of EDX was performed; further details follow in the subchapter Chemical composition.

In summary, the first look on surface morphology of the sample by the table SEM provided us some important information:

- the sample is charging while measured
- scratches are still present on the sample surface because of the imperfect polishing
- at least six different phases are present, while two of them are dominating
- the phase boundaries remind random growing of crystalline domain randomly oriented along the sample
- the chemical composition of the sample varies along the sample while closer to the sample edge

Because of the imperfect polishing we found by table SEM, the sample was polished once more by using diamond particles with diameter of 1 μm. Consequently, an advanced analysis utilizing FEI Quanta 200 E-SEM with field emission gun (FEG) was also performed. With FEG we achieve narrower electron beam and higher beam brightness. High-vacuum mode was also in use. The accelerating voltage for generating an electron probe was 25keV and the pressure was ~ 10^{-4} Pa in this case; similar to the previous analysis. The representative results are shown on Figure 6.
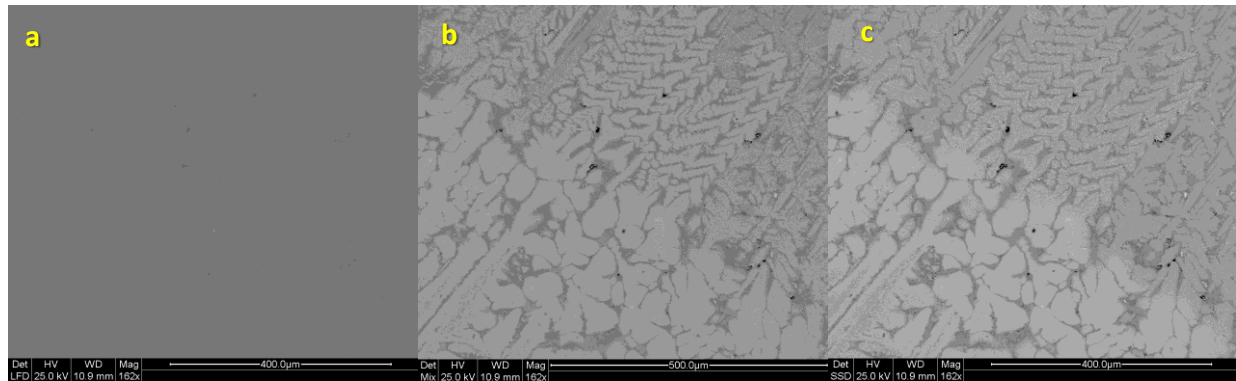

Figure 6 E-SEM pictures of expected ($Ti_{0.37}Zr_{0.37}Hf_{0.26}$)NiSn (a) morphology of the sample by using of SE detector (b) SE and BSE mixed picture (c) chemical composition along the sample by using of BSE detector.

From figure 6a we can see the perfectly flat homogenous surface without any defects (achieved by the successful polishing) taken in the intermediate area of the sample obtained in the secondary electron mode. SEs are mainly signals for surface topographic images, they are low energy electrons (10-50eV) as compared with incident electrons, and can only escape from a volume near the surface with a depth of 5-50nm. In (b) and (c) we can also see the differences in the chemical compositions along the sample. That confirmed us the presence of a multiphase product, as we noticed by the table SEM. The consideration based on the observed morphology says us the domains aren't growing randomly. Based on the observed structure in figure 6b and 6c we can state the fact that there occurs the long range order reminding the lamellar grow of the dominating phases in the dendrite shape as we have seen by the Nomarski microscopy.

Figure 7 shows the overviewing picture having noticeable middle section as well as the downer edge of the sample. This picture again confirms that the phase distribution varies along the sample – we can see the differences at the top and bottom region. It could be explained by the fact that the sample was cooled down during the synthesis from just one side and it caused different phase-forming conditions for different sections along the sample.
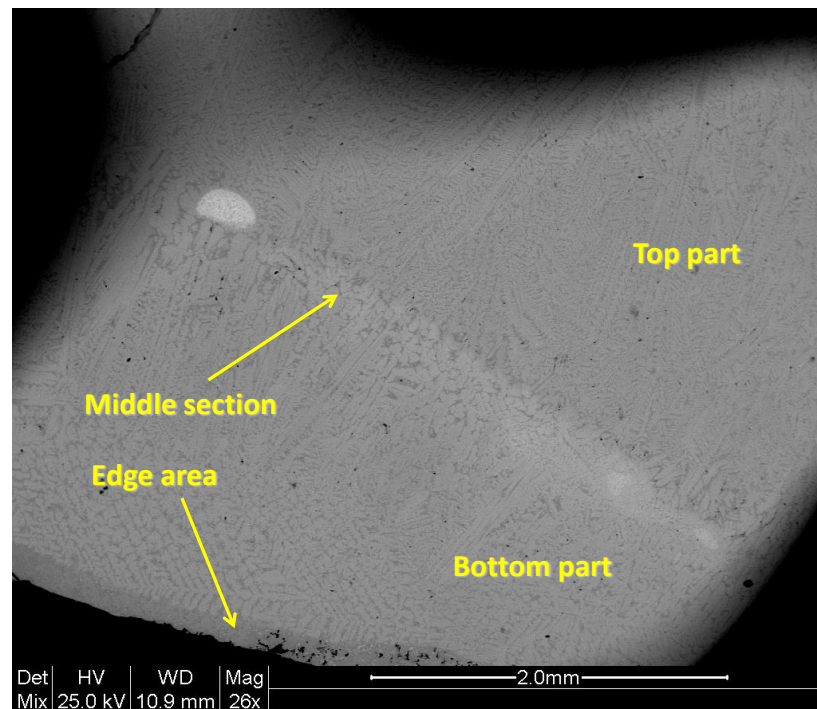
Top part

Middle section

Edge area

Bottom part

2.0mm

Figure 7 E-SEM pictures of expected (Ti$_{0.37}$Zr$_{0.37}$Hf$_{0.26}$)NiSn sample by using the mix of SE and BSE detectors -overview of the whole sample with the noticeable difference along the downer edge and also in the middle area.

The E-SEM microscopy confirmed the ideas from the table SEM – having six different phases, while the chemical composition and structure varies along the sample. However, the arrangement cannot be considered random - we can see very well defined areas with the lamellar grow – in the shape of dendrites. We can also state having three different regions – the top part, the bottom part and also the edge of the sample. All phases are having similar structure patterns along themselves, but differ for each region. We see that the top part seems to be richer for heavier elements (darker areas), and also the arrangement of dendrites seems to be denser (more dendrites per unit of surface area) than in the bottom part. On the other hand, the bottom part which is most probably richer for lighter elements and shows a very well defined lamellar arrangement as well. Between those two regions, an intermediate area is observed having composition of both and forms a visible gap. The sample bottom-edge is again noticeable significant difference in the chemical composition and a phase arrangement difference.

In order to specify the chemical composition of each phase, EDX analysis was consequently performed (as in the case of the table SEM) - details follow in the subchapter Chemical composition analysis.

Chemical composition analysis

Energy dispersive X-ray analysis (EDAX)

In this section, results of the EDX analyses performed either in the table SEM or E-SEM are presented. The output information is the spectrum of characteristic X-ray lines belonging to the detected elements across the X-ray energy range [vii]. Usually, also the SEM picture containing information about the element contrast is attached to each EDAX spectrum while showing the analyzed area. Two different modes were used for the chemical analyses – spot scan analysis (E-SEM), and selected area analysis (table SEM). It is necessary to note that the information depth

varies with the material density and the energy of incident electron beam. Therefore we should tkae this fact into our further consideration.

The surface area scan was performed first, in order to get an overview and average composition along our sample. Consequently, the spot analyses were performed for each present phase and the unique chemical composition of each phase was determined.

Selected area analysis

As noted previously, the basic Table Top SEM with the W-thread as an electron source having the accelerating voltage 15 keV and the EDAX detector was used for this analysis. The overviewing EDX spectrum and the analyzed area are shown on figure 8 and 9.
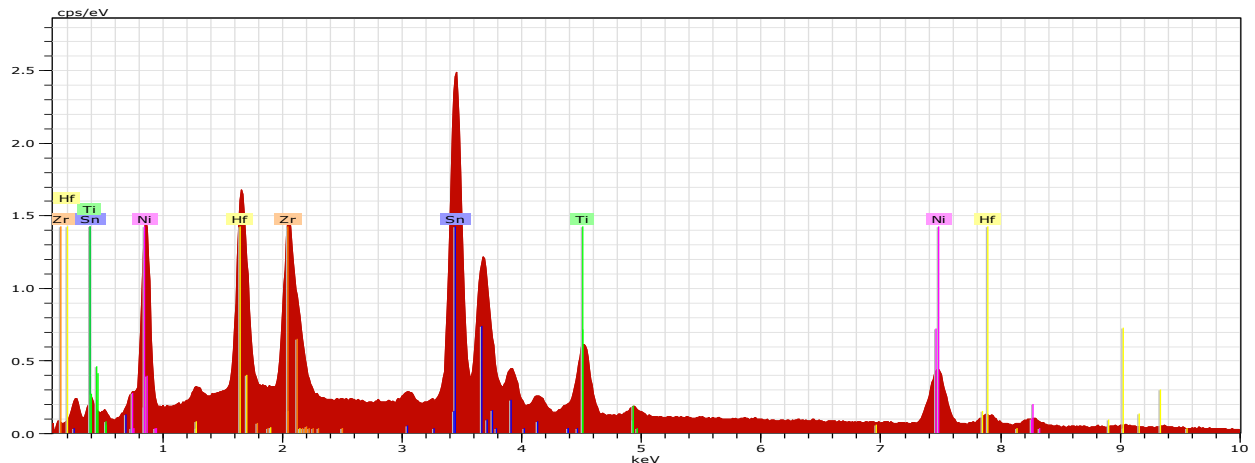
Figure 8 Overviewing EDX spectrum with identified peaks belonging to the expected elements: Ti, Zr, Hf, Ni and Sn.
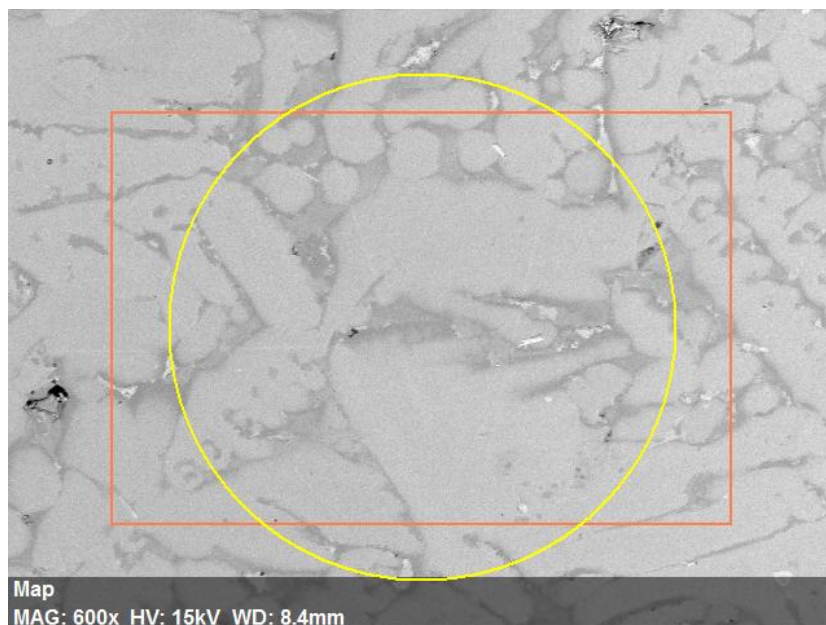
Figure 9 Selected area for EDX analysis in the orange box.

As we can see from figure 9, the scanning area contains of many different phases –black areas, dark and light grey, also something in between, as well as few white spots. Based on figure 8 we identified the presence of following elements: Ti, Zr, Hf, Ni and Sn – which confirms our expectations.

The good shaped peaks (belonging either to the K or L shell) were selected and the quantitative analysis was done based on the peak intensities. The results are displayed in Table 1. The selected area and the calculated values in Table 1 doesn't fit very well for ideal Half-Heusler alloy having the composition 12.2 % of Ti, 12.2 % of Zr, 8.9 % of Hf, 33% of Ni and 33% of Sn in atomic %. However, we are definitely having some Half-Heusler alloy with unexpected composition. The values point out the scan was taken in the area having most probably the Half-Heusler alloy poor for Hf (darker areas) and rich for Ti and Zr.

Table 1 The quantitative analysis of selected area – average chemical composition

Element	Atomic number	Series	Atomic concentration [at. %]	Error [%]
Titanium	22	K	14.77	0.2
Nickel	28	K	28.68	0.5
Zirconium	40	L	14.99	0.5
Tin	50	L	36.25	1.2
Hafnium	70	L	5.31	0.3

The results of second selected area analysis are shown on figure 10. The EDX analysis was done for another area and the element map was generated in order to visualise the distribution of elements along the phase boundaries. As we can see, the elements usually occurs in pairs, which doesn't like to mix with each other as in the case of Ni and Si, or even more obvious case for Zr and Ti. Only Hf seems to be distributed almost homogenously along the whole area except for the darker Hf poor regions.
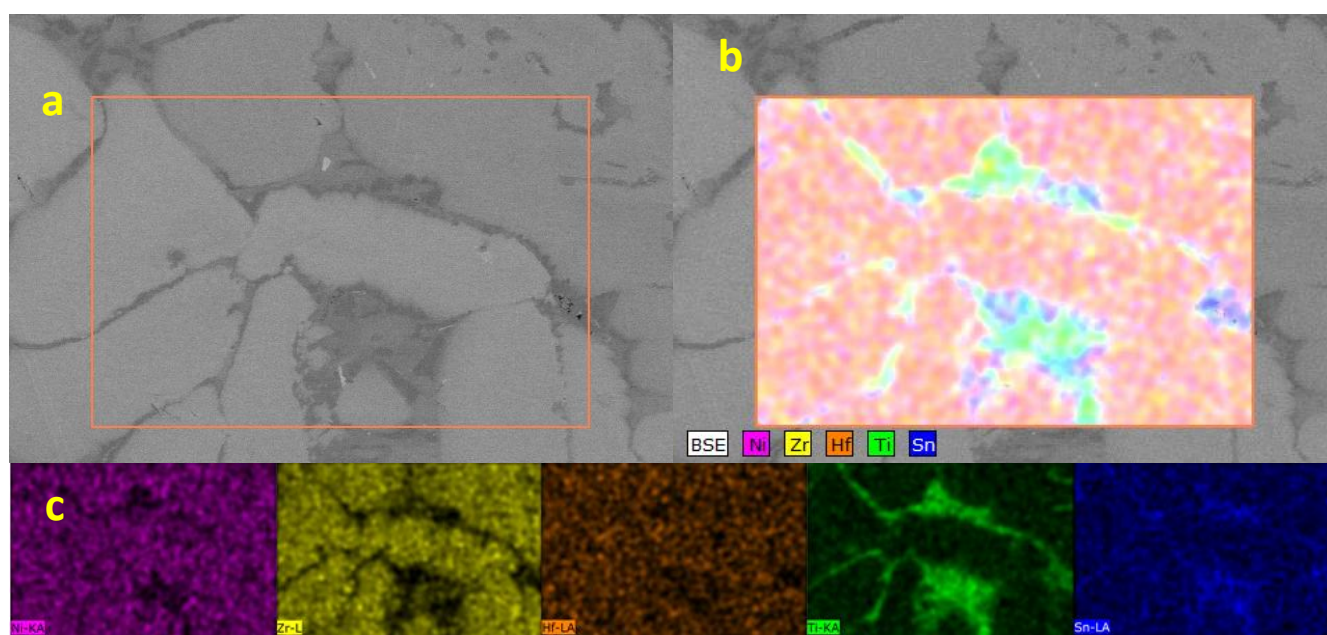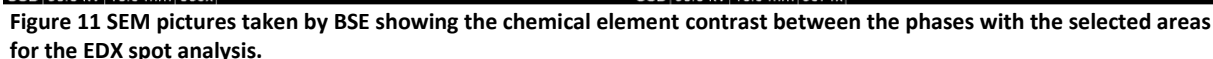

Figure 10 The element mapping of the selected area in the orange box; (a) the SEM picture of the selected area, (b) the element map containing all elements along the selected area and (c) single element maps for each detected element – purple Ni, yellow Zn, orange Hf, green Ti and blue Sn.

Spot scan analysis

In this section, the spot analysis (selected area having the diameter ~ 20 nm; depending on the impact electron beam focusing and its energy) of each detected phase was done and the chemical composition was listed for each phase. Each selected spot area where the EDX analysis has been done is shown on figure 11. For the quantitative chemical composition were always selected peaks belonging either to the K shell (Ti, Ni and Al) or L shell (Zr, Sn and Hf). The summarization of results of quantitative chemical composition analysis for each selected region corresponding to a present phase is noted in Table 2.

Figure 11 SEM pictures taken by BSE showing the chemical element contrast between the phases with the selected areas for the EDX spot analysis.

Nine different scans for determination of the chemical composition were performed in total. As we can see from the Table 2, The phase #4 and #8 has almost the same chemical composition, so they are most probably the same phase; being richer for Ni and poorer for Ti (both the lighter elements corresponding to the grey area). Phase #9 having high content of Al has to be removed from our consideration. Its presence needs to be explained by saying that we are having impurities. That also supports the fact of having very well defined black particle according to its shape.

In summary, we are having 7 phases with slightly different chemical composition. That confirms us the previous expectations based on the SEM morphology investigation of having at least 6 phases.

Table 2 Quantitative analysis of a spot area scan for nine different regions and the calculated chemical composition of each detected phase. Lowest and highest value for each element given in the green and red font.

	Phase #								
	1	**2**	**3**	**4**	**5**	**6**	**7**	**8**	**9**
Element	**Atomic % concentration [%]**								
Titanium	33.12	4.18	44.47	7.34	19.18	25.72	16.68	5.86	7.05
Nickel	13.15	36.85	11.25	37.38	13.28	35.32	12.56	36.73	43.29
Zirconium	11.40	11.13	6.28	12.38	14.95	4.24	16.13	13.78	2.62
Tin	13.14	31.14	34.74	30.78	13.75	32.29	12.40	32.23	15.08
Hafnium	29.19	16.71	3.26	12.12	38.84	2.43	42.23	11.40	2.32
Aluminium	-	-	-	-	-	-	-	-	28.57

The lists of suggested phases are as followed:

- #1 The white area in the middle of the black box. We expect to have the Hf rich phase in the middle of Ti rich phase with the average composition of $(Ti\ Zr_{0.35}Hf_{0.88})Ni_{0.4}Sn_{0.4}$

- #2 The light grey area. The Ti poorest phase (4.18 at. %) and also quite Ni rich phase while being quite rich for heavy Hf; having composition $(Ti_{0.13}\ Zr_{0.34}Hf_{0.51})Ni_{1.1}Sn_{0.94}$

- #3 The dark grey area. The Ti and also Si richest phase (44.47 at. % of Ti and 34.74 at. % of Sn), being poor for the Hf and Zr, and the poorest for Ni (11.25 at. %); having the composition $(Ti_{1.4}\ Zr_{0.19}Hf_{0.10})Ni_{0.34}Sn_{1.1}$

- #4 and #8 The middle grey area. The richest Ni phase (37.38 at. %), also Hf rich and Ti poor; having composition $(Ti_{0.22}\ Zr_{0.38}Hf_{0.37})Ni_{1.1}Sn_{0.93}$

- #5 Almost the lightest area. Very rich for Hf, Ti and Zr. On other hand, very poor for Ni and Si; having composition $(Ti_{0.58}\ Zr_{0.45}Hf_{1.2})Ni_{0.40}Sn_{0.42}$

- #6 The dark area of random shape. The poorest phase for heavy elements Zr and also Hf (4.24 at. % of Zr and 2.43 at. % of Hf), while being very rich for lighter Ti; having composition $(Ti_{0.78}\ Zr_{0.13}Hf_{0.07})Ni_{1.1}Sn_{0.98}$

- #7 The white area. The richest phase for Hf and Zr (42.23 at. % of Hf and 16.13 at. % of Zr), while being the poorest phase of Sn (12.40 at. %); having composition $(Ti_{0.51}\ Zr_{0.49}Hf_{1.3})Ni_{0.38}Sn_{0.38}$

In this section, we identified 7 different phases and determined the approximate chemical composition for each of them. The further specifications, as well as determination of most probable structures are followed in the next subchapter Crystal structure analysis.

Crystal structure analysis

In order to determine the crystal structure, the Powder X-ray diffraction (PXD) was used in our study. PXD is a typical laboratory characterization technique dealing with purity and determine lattice parameters and phase composition of synthesized crystalline solids. The output is a diffractogram; collection of diffracted intensity profiles as a function of the angle of incident beam. In principle, the incident X-ray radiation beam of characteristic wave length diffracts on randomly oriented crystalline grains of a powder sample, while following the Bragg equation for constructive interference of the radiation beams diffracted from a set of atomic planes *hkl*:

$$2d_{hkl}\sin(\Theta_{hkl}) = \lambda$$

There, λ is a wave length of the incident beam, Θ_{hkl} is the angle of incidence, d_{hkl} is spacing between the two parallel crystal planes [vii]. In our experiment, the Bruker D8 X-ray diffractometer, with CuKα radiation (λ =1.5418 Å) source, in the Bragg–Brentano geometry (the angle of incidence equals the angle of detection) was used, in the 2θ area 10-100 degrees.

Both samples were crushed by mortar and pestle to get fine powder. The fine powder was placed on the glass planar sample holder by the using of ethanol drop – to make the surface flat. Also the small amount of the Si standard was added as an inert standard material. Consequently, the two diffractions patterns were collected – for the untreated (sample 1) and annealed (sample 2)

compound. The analyzed diffraction pattern of the untreated $(Ti_{0.37}Zr_{0.37}Hf_{0.26})NiSn$ is shown on figure 12. The reflections were indexed and the phase composition was determined.
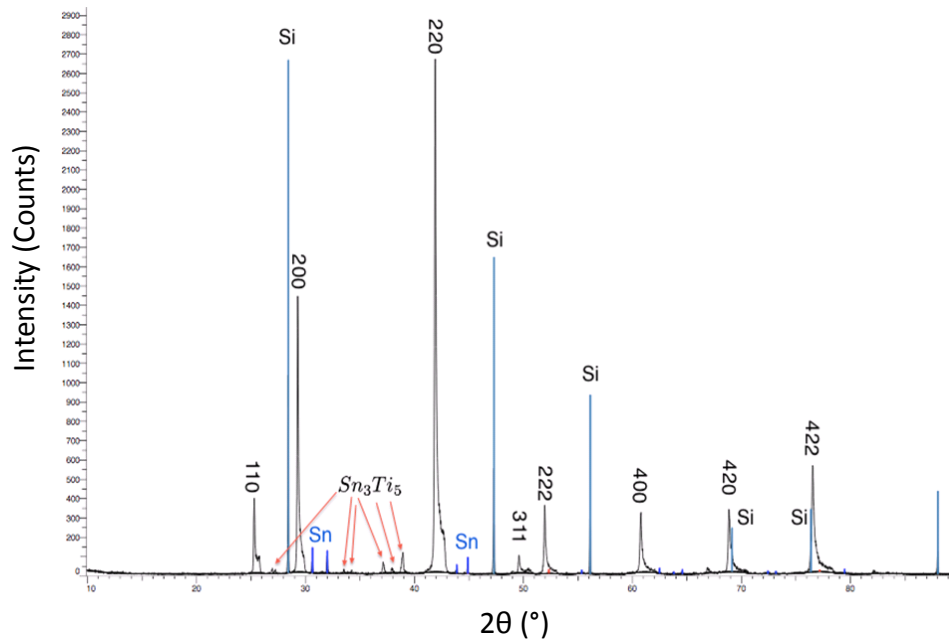

Figure 12 Diffraction pattern of the sample 1 with identified reflections.

After this analysis we can state the fact that we are having multiphase product. We identified the peaks belonging to the half-Heusler alloy (indexed peaks), standard silicon peaks, some peaks belong to the compound from the Pearson datasheet Sn_3Ti_5, and other peaks belongs to pure Sn. The peaks for the half-Heusler compound have noticeable shoulders. It says us, some slightly different half-Heusler phases are present in addition to main phase – they differ in the unit-cell size. The presence of shoulders on the right side of peaks (higher θ) based on the Bragg`s law points out that other phases have slightly smaller d. Because of that, they also have the smaller unit-cell. The detail view provided us the closer look upon the triple-peaks phenomena usual for our half-Heusler alloys. It also allows us to determine the *d*-parameter for each lattice; results are listed in Table 3.

Table 3 Calculated unit-cell parameters of three different phases.

Number of peak	d_1 [nm]	a_1 [Å]	d_2 [nm]	a_2 [Å]	d_3 [nm]	a_3 [Å]
#1	3,51547	6,08897	3,49406	6,05189	3,47333	6,01598
#2	3,04433	6,08866	3,02841	6,05682	3,00846	6,01692
#3	2,15262	6,08853	2,14139	6,05677	2,12760	6,01776
#4	1,83626	6,09019	1,82543	6,05427	1,81453	6,01812
#5	1,75795	6,08972	1,74849	6,05695	1,73729	6,01815
#6	1,52159	6,08636	1,51408	6,05632	1,50434	6,01736
#7	1,36108	6,08693	1,35451	6,05755	1,34540	6,01681
Average		6,08821		6,05623		6,01738
Deviation		0,00149		0,00223		0,00076

The largest unit-cell with the a-parameter $a_1 = 6,08821 \pm 0,00149$ has the Hf-richest dominating phase: because of the dominant presence of the largest Hf atoms in the structure. We can say the mixture of the #1, #5 and #7 phase, all rich for Hf contributes on the related peak intensity and the a value is average for all of them. For smaller half-Heuslers, it is also hard to identify precisely which phase contributes mostly. However, we can say the phases responsible for the shoulders (a_2 and a_3) should be the #2, #4 and #6 phases; the richest for the lighter and smaller elements. That caused the contraction in the unit-cell dimension. Phase #3 could be Sn_3Ti_5, surrounded by small amount of other elements also contributing on the average chemical composition.

The selected area of the diffraction patterns before (sample 1) in black and after the temperature treating (sample 2) in red is shown on figure 13.
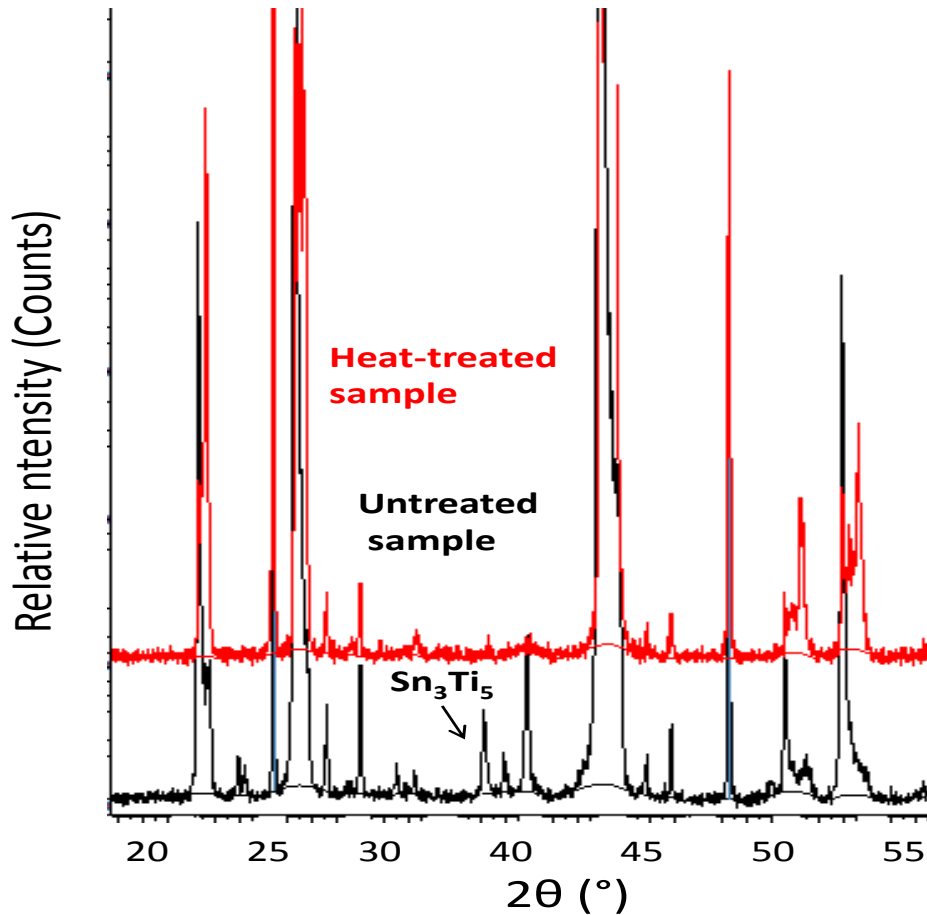

Figure 13 Untreated (black) and heat-treated (red) sample comparison.

It is obvious the heat-treated sample shows sharper localized peaks. The secondary phases are reduced in magnitude. Especially the density of secondary phase Sn_3Ti_5 was significantly reduced by annealing. This effect can be attributed to the dissolution of these domains into the half-Heusler matrix.

Conclusions

In order to the results we got in the morphology, chemical composition and crystal structure chapters, we can state the following:

- We identified up to 7 different phases present in the untreated sample; three dominating. The dendrite growth of those phases was observed

- The precise chemical composition of all phases present was determined

- X-ray diffraction studies confirmed us having of the half-Heusler alloys. We observed approximately three slightly different half-Heusler phases. Also the presence of Sn_3Ti_5 phase was observed

- The analysis of heat-treated sample pointed out the homogenous half-Heusler phase could be achieved: it is necessary to anneal the compound in the high temperature in order to obtain almost single phase product

In this report, we successfully analyzed the unknown sample by various techniques and determined precisely the half-Heusler alloy structure and its chemical composition, as well as the morphology.

[i] T.Graf et al./ Progress in Solid State Chemistry 39 (2011) 1-50.
http://www.sciencedirect.com/science/article/pii/S0079678611000021
[ii] S Populoh et al. SciVerse ScienceDirect. Scriopta Materialia 66 (2012) 1073-1076.
http://www.sciencedirect.com/science/article/pii/S1359646212001650
[iii] Naoki Shutoh, Shinya Sakurada. Journal of Alloys and Compounds 389 (2005) 204-208.
[iv] Jan-Willem G Bos and Ruth A Downie. Journal of Physics: Condensed Matter 26 (2014) 433201.
[v] F Casper et al. Semiconductor science and technology. 27 (2012) 063001.
[vi] Shuo Chen and Zhifeng Ren. Materials Today. Vol. 16, Number 10. October 2013.
[vii] Leng, Y. Materials Characterization: *Introduction to Microscopic and Spectroscopic Methods*. second ed. Weinheim, Germany: Wiley-VCH, 2013. Accessed May 16, 2015. http://dx.doi.org/10.1002/9783527670772.